Am J Physiol Heart Circ Physiol 308: H217–H231, 2015.
First published November 14, 2014; doi:10.1152/ajpheart.00469.2014.

A new hemodynamic model for the study of cerebral venous outflow

G. Gadda,[1] A. Taibi,[1] F. Sisini,[1] M. Gambaccini,[1] P. Zamboni,[2] and M. Ursino[3]

[1]*Department of Physics and Earth Sciences, University of Ferrara, Ferrara, Italy;* [2]*Vascular Diseases Center, University of Ferrara, Ferrara, Italy; and* [3]*Department of Electrical, Electronic and Information Engineering, University of Bologna, Bologna, Italy*

Submitted 8 July 2014; accepted in final form 10 November 2014

Gadda G, Taibi A, Sisini F, Gambaccini M, Zamboni P, Ursino M. A new hemodynamic model for the study of cerebral venous outflow. *Am J Physiol Heart Circ Physiol* 308: H217–H231, 2015. First published November 14, 2014; doi:10.1152/ajpheart.00469.2014.—We developed a mathematical model of the cerebral venous outflow for the simulation of the average blood flows and pressures in the main drainage vessels of the brain. The main features of the model are that it includes a validated model for the simulation of the intracranial circulation and it accounts for the dependence of the hydraulic properties of the jugular veins with respect to the gravity field, which makes it an useful tool for the study of the correlations between extracranial blood redistributions and changes in the intracranial environment. The model is able to simulate the average pressures and flows in different points of the jugular ducts, taking into account the amount of blood coming from the anastomotic connections; simulate how the blood redistribution due to change of posture affects flows and pressures in specific points of the system; and simulate redistributions due to stenotic patterns. Sensitivity analysis to check the robustness of the model was performed. The model reproduces average physiologic behavior of the jugular, vertebral, and cerebral ducts in terms of pressures and flows. In fact, jugular flow drops from ~11.7 to ~1.4 ml/s in the passage from supine to standing. At the same time, vertebral flow increases from 0.8 to 3.4 ml/s, while cerebral blood flow, venous sinuses pressure, and intracranial pressure are constant around the average value of 12.5 ml/s, 6 mmHg, and 10 mmHg, respectively. All these values are in agreement with literature data.

mathematical modeling; cerebral outflow; posture dependence; jugular veins collapse; collateral routes

THE EXTRACRANIAL VENOUS SYSTEM represents an important determinant of the brain circulation, but its role in the pathology of the central nervous system is not fully understood yet (4, 26). It is recognized that, in supine position, the jugular veins represent the main outflow route for the cerebral circulation (2, 6, 25, 36, 38), being able to carry most of blood flow from the brain and from other extracerebral territories (~700–720 ml/min; Refs. 27, 33) with respect to a cerebral blood inflow of ~750 ml/min (45). However, the jugular venous system exhibits important flow limitation during upright posture changes, because the jugular veins tend to collapse as a consequence of the decrease of transmural pressure due to the gravitational field, causing a significant increase in resistance (3, 7, 12, 14, 26). In the absence of other routes for extracranial outflow, this flow limitation would have dramatic effects on the cerebral circulation, since, apart from brief transient time intervals, the average cranial arterial inflow is expected to be equal to the cranial venous outflow for the mass preservation.

Address for reprint requests and other correspondence: G. Gadda, Dept. of Physics and Earth Sciences, Univ. of Ferrara, Via Saragat 1, 44122 Ferrara, Italy (e-mail: gddgcm@unife.it).

As a consequence, large attention has been devoted to the venous circulation in the upright state, in an effort to understand which alternative routes can carry the brain venous outflow. It has long been postulated that the vertebral venous system may provide an important alternative route for venous outflow when standing or sitting; this was first demonstrated with the use of contrast media in rhesus monkeys (9) and subsequently measured in humans with the Doppler and magnetic resonance imaging technique (2, 6, 7, 25, 38). Valdueza et al. (33) observed that blood flow in the jugular veins decreases from 700 ml/min in supine position down to 70 ml/min at 90° elevation, while blood flow in the vertebral veins raises from 40 to 210 ml/min.

Accordingly, a classical model of the cerebral venous outflow assumes the existence of two main alternative routes: a route through the jugular veins, with smaller resistance in supine conditions, and a parallel vertebral route with higher resistance. In upright conditions, when the first route collapses, blood flow is diverted to the second one. Based on this idea, Gisolf et al. (14) developed a mathematical model of cerebral venous outflow: the model consists of two jugular veins (each composed of a chain of 10 units with resistances and capacitances) and a vertebral plexus (described with a single resistance). The elements in the jugular veins collapse according to the "tube law" (3, 12) during a posture change but can reopen during a Valsalva maneuver. With this model, the authors studied how venous blood flow changes from supine to upright position and confirmed that the cerebral venous distribution depends on posture. Despite the previous pivotal studies, many aspects of the cerebral venous outflow system are still problematic.

First, it is well known that cerebral autoregulation maintains blood flow to the brain quite constant, despite pressure changes (1, 21): this signifies that an amount of blood flow much greater than that measured in the vertebral system must be carried out in the upright state. This discrepancy was clearly recognized by Valdueza et al. (33) who observed that "a mean difference of about 450 ml/min remained." These authors hypothesized that other routes, such as the epidural veins, significantly contribute to the orthostatic venous outflow.

Second, some authors, using the color Doppler technique, recently observed that blood flow along the jugular veins in upright conditions is not longitudinally constant but increases progressively when the measurement site is moved from the upright sections (close to the jugular foramen into the skull) to the downstream sections (close to the subclavian vein) (6, 28, 41, 44). This observation supports the idea that additional anastomotical routes carry part of the cranial blood flow to the jugular veins even in upright position, bypassing the upstream more collapsed sections. In fact, as a consequence of the different effect of gravity, only the higher portions of the

jugular veins are probably fully collapsed, whereas the downstream sections are opened. A comprehensive model of the cerebral venous outflow should also include these further collateral routes.

Due to the complexity of the relationships involved, and the large variability in the anatomical parameters, it is extremely difficult to understand the effect of alterations in the extracranial venous circulation in simple qualitative terms. The study of the cerebral venous outflow, and of its implications in healthy and diseased conditions, can largely benefit from the use of computational models.

So far, most models of the cerebral circulation focused on the intracranial circulation and on its control mechanisms, by providing just a very simplified description of extracranial venous return. A notable exception is the model by Gisolf et al. (14) mentioned above, which, however, includes only the vertebral plexus as an alternative drainage pathway.

The aim of the present study is to develop and validate a comprehensive original lumped parameter model of the cerebral venous outflow system, which overcomes some of the limitations noticed above. In particular, compared with the model by Gisolf et al. (14) the present model also includes:

1) An accurate model of the intracranial circulation developed in past years, which incorporates the autoregulation of cerebral blood flow (13, 30, 32). This model provides the correct values of cerebral blood flow to the venous return model. Moreover, it allows a quantitative analysis of the effect of alterations in the venous pathways on intracranial quantities, such as the effect on intracranial pressure, venous sinuses pressure, capillary pressure, and cerebrospinal fluid circulation.

2) A more sophisticated description of the collateral pathways, including not only the vertebral plexus but also other anastomoses leading blood to the downstream sections of the jugular veins (6, 28, 41, 44).

In the following, the model is described qualitatively, with emphasis on the new aspects, and parameters are given in accordance with the physiology. All equations are presented in the APPENDIX. The model is validated against results in the literature, concerning the effect of a posture change in healthy subjects; a sensitivity analysis is also performed to clarify the role of the alterations in some parameters.

The model may represent an useful tool for the study of the correlation among posture variations, vessel conductances (normal or abnormal), and the consequent pressure and flow changes. This may have a great impact toward a deeper understanding of pathological disorders involving abnormalities of the cerebral venous outflow. In perspective, it may be used to assess which alterations in the extracranial venous outflow may be in relation with central nervous system disorders and aging (6, 10, 24, 40, 42).

MATERIALS AND METHODS

Model Description

Our mathematical model for the simulation of the head and cerebral circulation and drainage system includes two submodels built using lumped parameter method. The model is represented in Fig. 1.

Mathematical models may represent an useful tool for improving comprehension of complex systems like this, describing the behavior of a real process using a system of equations (14, 20, 22). What we are developing is a lumped parameter model, i.e., a model in which the continuous variation in space of the state variables of the system is represented by a finite number of variables (35). In other words, a lumped parameter model allows the description of spatially distributed physical systems to be simplified using a network of discrete entities that approximate the real system. The use of a lumped parameter model presents a significant advantage since it exhibits a small number of parameters able to account for an entire physiological or clinical phenomenon in a concise way. This fact improves the clinical meaning of the results obtained: the behavior of the model can be studied more easily than the system that it represents.

Every segment x of Fig. 1 consists of a capacitor C_x that simulates the property of the segment to accommodate volume and of a conductance G_x that simulates the property of the segment to drain blood.

All the model equations are presented in the APPENDIX.

The mathematical model of the cerebral hemodynamics, enclosed in the "BRAIN" dashed rectangle of Fig. 1, has been fully developed and validated by Ursino and colleagues in previous works (13, 30, 32). This model simulates the hemodynamics of the arterial-arteriolar and venous cerebrovascular bed, the cerebral arterioles regulation mechanisms, the cerebrospinal fluid production and reabsorption processes, the Starling resistor mechanism for the cerebral veins, and the nonlinear pressure-volume relationship of the craniospinal compartment.

The structure of the cerebral venous outflow model (shown in Fig. 1 out of the "BRAIN" dashed rectangle) has been developed starting from a recent work of Zamboni et al. (44). The main part of the model is composed of four venous ducts: two internal jugular veins (IJVs; left and right) and two vertebral veins (VVs; left and right). The internal jugular veins are modeled by dividing them into three segments with different conductive and capacitive values, to better implement the different biomechanical properties of these vessels along their length and to better simulate the effect of hydrostatic pressure gradient in upright position.

Indeed, jugular veins are collapsible blood vessels characterized by marked changes in their cross-sectional configuration depending on transmural pressure $P_{xint} - P_{xext}$ (26). The latter is affected by hydrostatic pressure gradient during a posture change (7). On the other side, the hydrostatic pressure gradient does not significantly affect the lumen of the vertebral veins.

Anatomically speaking, left and right lower jugular segments (J1) correspond to the segments close to the junction of the internal jugular veins with the subclavian vein, at the confluence with the brachiocephalic vein trunk. The middle segments (J2) correspond to the point where the veins are in an anatomical relationship with the more lateral contour of the thyroid gland. The upper segments (J3) correspond to the point before the passage through the jugular foramen into the skull (43).

To account for the growth of blood flow from J3 to J1 (6, 8, 10, 28, 33, 41, 44), we must consider that a quota of the head inflow is conveyed into the internal jugular veins more caudally with respect to the J3 position, through intra- and extracranial anastomosis. To account for this experimental evidence, the model is developed so that the two jugular veins are linked by a network of eight constant conductances and two constant capacitors that simulate the presence of collaterals and anastomotic connections. This collateral network also allows the drainage of the extracranial venous blood, i.e., of that part of blood coming from the two external arteries to serve the head organs and tissues out of the braincase (44).

In the model, the conductance of the external arteries (i.e., the conductance of the tract with blood flow Q_{ex} in Fig. 1) has been maintained constant. Conversely, as described in previous works (30) and explained through *Eqs. 7–11* in the APPENDIX, the conductance of the intracerebral arterioles is subjected to autoregulatory mechanisms, which work to maintain quite a constant cerebral blood flow despite moderate changes in cerebral perfusion pressure. The choice of a constant extracranial conductance can be justified by the observation that autoregulation in extracranial vessels is generally weak and slow. Moreover, during hypotension a vasoconstriction of baroreflex origin

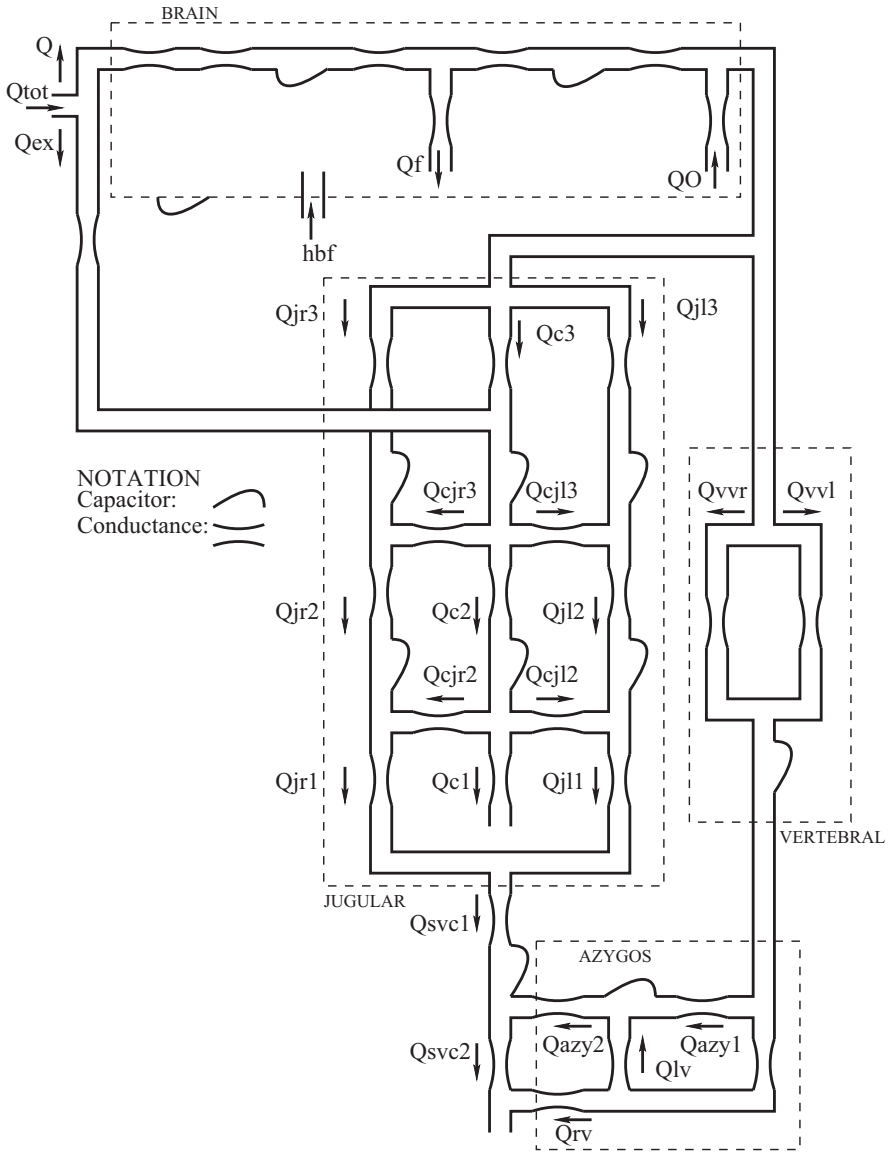

Fig. 1. Scheme of the lumped parameter model for the study of the cerebral venous outflow. The "BRAIN" box represents the intracranial part of the model, already developed in the work of Ursino et al. (13, 30, 32). Outside the "BRAIN" box there is the extracranial part of the circuit that has been developed starting from the work of Zamboni et al. (44).

may counteract this weak vasodilatory autoregulation, thus resulting in negligible conductance changes.

We assume that, in the basal supine condition, the anastomotic upper connection c3 is latent: blood flows in it only when the posture is upright or when there is a lack of drainage in one vessel tract, or more than one.

Moreover, a basic submodel of six constant conductances and three constant capacitors is implemented in the main model to describe the lumbo-azygos system (AZY), which links jugular and vertebral pathways at the level of superior vena cava (36).

The model is made up of several differential equations. Every equation links together the elements representative of a specific point x (i.e., pressure P_x, conductance G_x, and capacity C_x) with the elements representative of the other segments of the system to account for mass preservation and to include effects due to posture changes. We report here (*Eqs. 1* and *2*) examples of the two types of equations used to built the cerebral venous outflow model.

Equation 1, one of the state equations of the model listed in the APPENDIX, implements the mass preservation. We can see how the pressure at a given point (jr3 in this example) is related to capacity, conductances, and drops of pressure.

$$\frac{dP_{jr3}}{dt} = \frac{1}{C_{jr3}}\left[\left(P_{vs} - P_{jr3}\right)G_{jr3} - \left(P_{jr3} - P_{c3}\right)G_{cjr3} - \left(P_{jr3} - P_{jr2}\right)G_{jr2}\right] \quad (1)$$

To include dynamics due to posture changes from supine to upright in the gravity field, conductances in the jugular veins are modeled using a nonlinear relation (*Eq. 2*) with switch-like properties so that for negative or low transmural pressure $P_{xint} - P_{xext}$ at a given point x, the related vessel conductance G_x is low, while for high transmural pressure, vessel conductance approaches a maximum value (14).

$$G_x = k_x\left[1 + \left(\frac{2}{\pi}\right)\arctan\left(\frac{P_{xint} - P_{xext}}{A}\right)\right]^2 \quad (2)$$

The effect of hydrostatic pressure gradient is hidden in the internal pressure P_{xint}. The value of this pressure decreases by a factor ρgh during the transition from supine to standing position. Obviously, the collapse of the upper segment of the jugular veins (J3) is more pronounced with respect to the lower segments (J1), due to the presence of the height h. We use the superior vena cava as the zero level for the hydrostatic pressure.

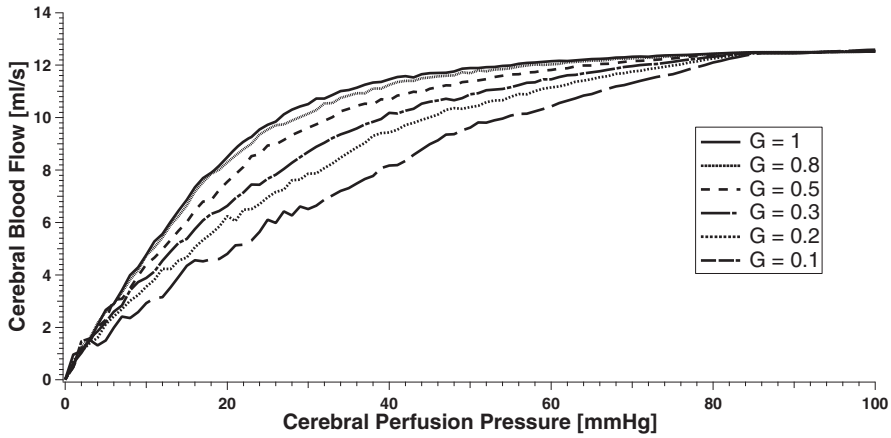

Fig. 2. Curves of the cerebral blood flow vs. cerebral perfusion pressure for maximum ($G = 1$) and progressive impaired autoregulation gain.

To solve the whole system of equations we resort to an algorithmic approach. We used the software package Berkeley Madonna (free available version beta 9.0.111; Ref. 17a), developed on the Berkeley campus under the sponsorship of National Science Foundation and National Institutes of Health and widely used in biology and biological engineering (11, 15). The package provides three fixed-stepsize integration methods and two variable-stepsize integration methods. We chose the iterative method Runge-Kutta 4 to perform all the computations. The algorithms used by Berkeley Madonna are derived from the routine methods published in the series of books *Numerical Recipes* (23).

Assignment of Basal Parameters

We adjusted every parameter value in search of agreement between model simulations and measurements that can be obtained from literature results. Starting from the work on the intracranial circuit already developed by Ursino and Lodi (30), we moved around several literature data to choose the right inputs for the jugular-vertebral network, adopting reasonable criteria to determine parameters not available from literature.

Parameters were assigned on the basis of the following criteria:

1) All parameters concerning the intracranial circulation were given the same values as in the previous works (30, 32), where a thorough justification can be found. Briefly, intracranial vascular resistances and capacities were assigned on the basis of physiological and anatomical data on brain hemodynamics in a normal subject. The autoregulation gain and time constants were given to simulate the typical autoregulation response of an healthy individual who exhibits mild cerebral blood flow changes despite cerebral perfusion pressure changes (see Fig. 2). Parameters summarizing the cerebrospinal fluid circulation and intracranial compliance were set to establish a normal hydrodynamics, as derived from infusion or PVI tests in the neurological literature. All the intracranial basal parameters are summarized in Table 1.

2) The values of all conductances in the extracranial circulation were assigned starting from physiological values of pressures and flows (see Tables 2 and 3, respectively). In particular, as shown in Table 2, we assumed a progressive pressure reduction from the venous sinuses to the right atrium (i.e., the central venous pressure), assuming normal values as large as 6 and 5 mmHg, respectively. Typical average values reported in Table 2 are assigned as basal values to the pressure of the superior tract of collateral P_{c3}, of venous sinuses pressure P_{vs} (30), and of central venous pressure P_{cv} (14). Intermediate basal pressure values (P_{jr3}, P_{jr2}, etc…) are assigned to simulate a homogeneous pressure drop along the whole circuit from the exit of venous sinuses to the vena cava. External pressure P_{xext} to the upper sections of the jugular veins J3 and J2 is set to zero, while at the lower segments J1 is set to the average thoracic pressure during a complete respiratory cycle (18). Looking at the basal flows shown in Table 3, cerebral blood flow Q is the total blood volume entering the cranial cavity per unit time (45). At the exit from the skull, it is drained both by jugular and vertebral veins, with the two jugular veins that contribute to drain the main part of blood only in supine position. The flow through left and right external carotid arteries Q_{ex} is set according to the data of Yazici et al. (37) and taking into account the lower cerebral flow reported by these authors (i.e., we assumed the same ratio between the extracranial carotid blood flow and blood flow in the common carotid artery as in Ref. 37). It is also assumed that 40% of this flow is directed to every jugular via the anastomotic connections, while the remaining blood is drained down through the middle collateral. Finally, half of the vertebral flow enters in the azygos vein, while the other half is divided between lumbar vein duct (1/3 of the total) and renal vein duct (2/3 of the total).

3) The values of the capacities in the extracranial circulation (Table 4) have been determined using the following considerations:

i) Capacities in the jugular tracts and in the vertebral veins have been computed from the values of transmural pressures, lengths, and areas reported in the literature (33) and assuming a negligible unstressed volume (i.e., we consider an average capacity, quite independent of transmural pressure).

Table 1. *Basal values of quantities related to the intracranial circuit (supine condition)*

Quantity	Value
C_{pan}	0.205 ml/mmHg
ΔC_{pa1}	2.87 ml/mmHg
ΔC_{pa2}	0.164 ml/mmHg
G_{aut}	3
k_E	0.077 ml^{-1}
k_R	13.1 $\times$ 10^3 $mmHg^3 \cdot s \cdot ml^{-1}$
k_{ven}	0.155 ml^{-1}
P_a	100 mmHg
P_{icn}	9.5 mmHg
P_{pa}	58.9 mmHg
P_v	14.1 mmHg
P_{v1}	−2.5 mmHg
P_{vs}	6 mmHg
Q_n	12.5 ml/s
R_0	526.3 $mmHg \cdot s \cdot ml^{-1}$
R_f	2.38 $\times$ 10^3 $mmHg \cdot s \cdot ml^{-1}$
R_{la}	0.6 $mmHg \cdot s \cdot ml^{-1}$
R_{pv}	0.880 $mmHg \cdot s \cdot ml^{-1}$
R_{vs1}	0.366 $mmHg \cdot s \cdot ml^{-1}$
τ_{aut}	20 s
x_{aut}	2.16 10^{-4}

Table 2. *Basal values of pressures related to the jugular-vertebral circuit (supine condition)*

Pressure	Symbol	Value, mmHg
At the collateral (superior tract)	P_{c3}	6.00
At the right jugular (superior tract)	P_{jr3}	5.85
At the left jugular (superior tract)	P_{jl3}	5.85
At the collateral (middle tract)	P_{c2}	5.85
At the vertebral vein	P_{vv}	5.80
At the right jugular (middle tract)	P_{jr2}	5.70
At the left jugular (middle tract)	P_{jl2}	5.70
At the azygos vein	P_{azy}	5.50
At the superior vena cava (superior tract)	P_{svc1}	5.40
At the superior vena cava (inferior tract)	P_{svc}	5.20
At the right atrium (central venous pressure)	P_{cv}	5.00
External at J3 and J2	P_{xext}	0
External at J1	P_{xext}	−6.50

ii) Capacity of the azygos veins are assumed comparable to the capacity of the vertebral veins.

iii) Capacities of the collateral tracts have been computed, in the absence of clear geometrical data, by assuming that they are approximately proportional to the square root of conductances and using the capacities of the jugular tracts as a reference.

iv) A small value has been given to the capacity of the venous sinuses, since most of these vessels are surrounded by the dura mater.

v) We checked that, with the previous choices, the overall capacity of the venous outflow circulation is close to the value used in Ursino and Magosso (31) for the capacity of the cerebral venous vascular bed (10.7 ml/mmHg).

4) To complete the determination of model parameters, we need to assign a value to A and k_x in the equations describing the conductance of the jugular veins (*Eq. 2*). These values have been given to address two major requirements:

i) In supine position, conductances must assume a constant value in accordance with the linear relationship between drops of pressure and flows and in accordance with the values reported in Tables 2 and 3.

ii) In upright position, the conductance changes induced by venous collapse (consequence of the hydrostatic pressure gradient) determine a redistribution of blood flow from the jugular veins to the vertebral-azygos complex and the collateral route. These changes have been assigned to simulate typical values of jugular blood flow and vertebral blood flow reported in Ref. 33.

It is worth noting that the last criterion is the only a posteriori information that we used in assigning parameters: all other information was set a priori, i.e., was independent of the results obtainable during posture changes. However, we did not use an automatic procedure to assign these parameters but just a manual adjustment to verify reasonable agreement between model blood flow changes and literature data. Since A and k_x were assigned using a posteriori information, we subsequently checked that the conductances vs. transmural pressure curves so obtained for each jugular tracts are in reasonable agreement with our knowledge on the biomechanics of compressible vessels. These curves, reported in Fig. 3, show that the collapse initiates at a transmural pressure approximately as high as 1–2 mmHg and is almost completed at moderate negative transmural pressure values in agreement with the literature information (5, 14, 16).

Table 3. *Basal values of flows related to the jugular-vertebral circuit (supine condition)*

Flow	Symbol	Value, ml/s
At the brain (cerebral blood flow)	Q	12.50
At every jugular vein	Q_{jr3} and Q_{jl3}	5.85
At every vertebral vein	Q_{vvr} and Q_{vvl}	0.40
At the external duct (face and neck)	Q_{ex}	5.00
At every anastomotic connection	Q_{cjr3}, Q_{cjl3}, Q_{cjr2}, Q_{cjl2}	1.00
At the middle collateral	Q_{c2}	3.00
At the azygos vein	Q_{azy1}	0.40
At the lumbar vein	Q_{lv}	0.13
At the renal vein	Q_{rv}	0.27

Table 4. *Capacities related to the jugular-vertebral circuit (supine condition)*

Capacity	Symbol	Value, ml/mmHg
At the venous sinuses	C_{vs}	0.5
At the right jugular (superior tract)	C_{jr3}	1.0
At the left jugular (superior tract)	C_{jl3}	1.0
At the right jugular (middle tract)	C_{jr2}	2.5
At the left jugular (middle tract)	C_{jl2}	2.5
At the central collateral (superior tract)	C_{c3}	0.7
At the central collateral (middle tract)	C_{c2}	1.4
At the superior vena cava (lower tract)	C_{svc}	20.0
At the azygos vein	C_{azy}	0.5
At the vertebral vein	C_{vv}	0.5

In the current model the value of the parameter A is 0.8, while we assigned to k_{jr3}, k_{jr2}, and k_{jr1} the value of 11.0, 13.0, and 6.9, respectively (the same values are assigned to the left coefficients k_{jl3}, k_{jl2}, and k_{jl1}). By choosing these parameters, Fig. 3 shows the relation between conductance of the jugular segments and the transmural pressure.

RESULTS AND DISCUSSION

Once we verified that the model, with basal parameter values, can simulate the main blood flow changes from supine to upright position, we performed a sensitivity analysis on some model parameters. We focused our attention on changes in conductances in the venous pathways. Indeed, analysis of the correlation between conductances and posture variation and the subsequent pressures and flows changes might give information about the parameters that have greater impact on intracranial hemodynamics (and then on related disorders). From our particular point of view, analysis of the results before and after the variation of a conductance is meaningful, since it provides information on how the closure of a particular drainage tract affects important physiological parameters, such as venous sinuses pressure P_{vs} (and so intracranial pressure P_{ic} and cerebral circulation) or flows in the jugular and vertebral veins (Q_{svc1} and Q_{vv}, respectively). For simplicity, we focused only on the right conductance variations, since analysis on left conductance variations will be symmetrical.

Each conductance under examination was varied from the baseline value, that is representative of physiological condition, to zero value that simulates total absence of drainage from a section of the network; simulations of posture variation were performed in both situations.

Once we performed the sensitivity analysis by setting one conductance to zero, we chose to simulate total and halved occlusions of more than one drainage tract at the same time, following the typical patterns reported in Zamboni et al. (39). This work is one of the recent studies concerning the relations among the main cerebral venous outflow routes, their disorders, and the occurrence of neurological diseases (10, 17, 19, 28, 29, 34).

Simulation results of particular interest are shown in the following.

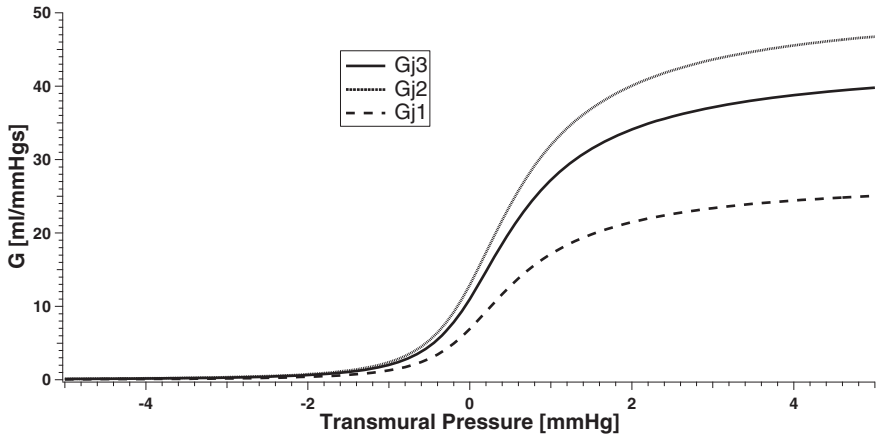

Fig. 3. Characteristic curves of the conductance (*G*) vs. transmural pressure in each jugular segment.

Simulation with Basal Parameter Values

Figure 4 shows how the model simulates the total amount of jugular flow Q_{j3} and vertebral flow Q_{vv} at the equilibrium in both supine and upright conditions. Results are also compared with the experimental mean flows reported in Valdueza et al. (33). The very good agreement between simulated supine and upright flows and experimental results means that parameters of the model are well assigned.

In Fig. 5, we show the behavior of the simulated venous sinuses pressure P_{vs} over time when passing from supine to upright condition. When basal parameters are used, our model predicts an increase of 2.68 mmHg (from 6.00 to 8.68 mmHg) with change of posture. It also predicts that P_{vs} needs ~3 s to reach the upright equilibrium.

In Fig. 6, the behavior of the simulated right jugular flow Q_{jr3} and right vertebral flow Q_{vvr} over time is reported in the same conditions of Fig. 5. For simplicity, we focus the attention only on the right jugular and vertebral flows, since results on left vessels are symmetrical. Figure 6 shows that our model predicts a strong decrease of the right jugular flow Q_{jr3} when changing from supine to upright (from 5.87 to 0.69 ml/s). Conversely, flow at the right vertebral vein Q_{vvr} rises from 0.40 to 1.70 ml/s during the change from the supine to upright condition. Figure 6 also shows that upright Q_{jr3} and Q_{vvr} flows reach their equilibrium with different behaviors.

In these conditions the flow through jugular and vertebral veins is equally distributed between left and right side. The collateral tract c3 is latent in supine position, while in upright it drains the amount of blood that does not flow through jugular or vertebral veins (~7.7 ml/s).

Figure 7 summarizes amounts of simulated total inflow Q_{tot}, flow to face and neck Q_{ex}, cerebral blood flow Q, and total jugular, vertebral, and collateral flows at equilibrium (Q_{j3}, Q_{j2}, Q_{j1}, Q_{vv}, and Q_{c3}) in supine and upright conditions.

We see that Q_{tot} is the sum of Q_{ex} and Q. Moreover, the histogram shows the different type of drainage the cerebral blood flow Q undergoes in supine and upright position. These different blood distributions are due to the changes in jugular conductances that occur when upright position is simulated (*Eq. 2*).

Results can be summarized as follow. Cerebral blood flow Q remains substantially constant despite the posture change, as a consequence of the action of autoregulatory mechanisms. In fact, the moderate increase in venous sinuses pressure lies well inside the autoregulatory range (30). Blood flow Q_{j3} in the upper portion of the jugular vein exhibits a dramatic fall in the upright state: most of the cerebral blood flow passes through the collateral route c3. Moreover, blood flow in the vertebral veins Q_{vv} increases by about four times. These results agree with those reported in literature (33). Furthermore, blood flow in the jugular veins progressively increases from J3 to J1, since part of blood flow is drawn from the collateral route to the jugular tract via the anastomoses cj3 and cj2 (see Fig. 1). The reason is that the last portion of the jugular veins exhibits a less pronounced collapse in upright condition compared with the first tract, due to a

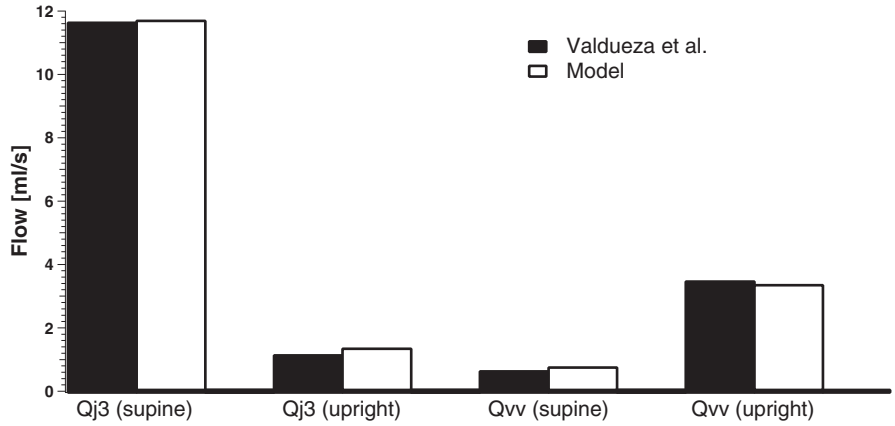

Fig. 4. Comparison between literature flow data (33) and model outcome.

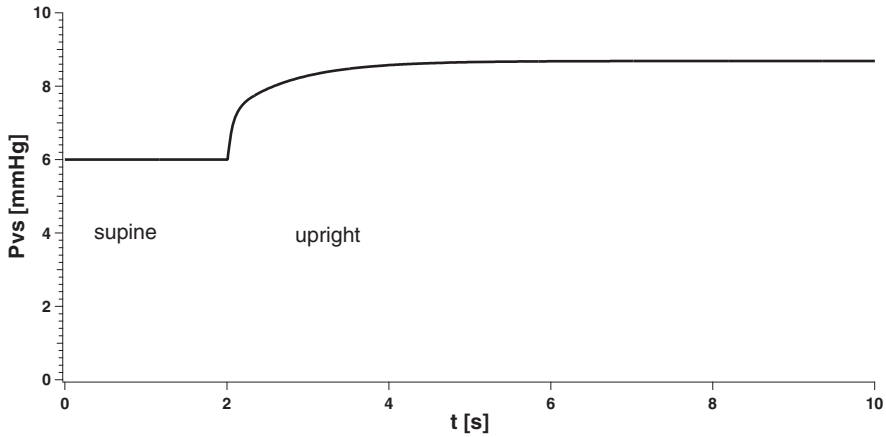

Fig. 5. Venous sinuses pressure (P_{vs}) behavior over time in supine and upright simulations.

smaller gravitational pressure gradient and due to the effect of the negative intrathoracic pressure.

Sensitivity Analysis

To clarify the role of the main routes involved in cerebral venous outflow, and a possible effect of a pathological alteration, we performed a thorough sensitivity analysis. It consists of two steps:

1) We first interrupted blood flow in a single route by assigning a zero value to the corresponding conductance and checked the effect in steady-state conditions.

2) Then, we simulated four typical pathological alterations already reported in the clinical literature (39) and characterized by a conductance reduction in multiple venous paths.

Effect of a single closure. Results are summarized in Figs. 8, 9, and 10 with regards to the effect of a single closure on venous sinuses pressure P_{vs}, outflow from the confluence of the two jugular veins Q_{svc1} and vertebral blood flow Q_{vv}, respectively. Results show that the cerebral venous outflow system is quite robust in response to a single vessel closure, both in supine and upright conditions. This signifies that interruption of a single path can be quite easily replaced by an alternative route. Pressure P_{vs} at the venous sinuses, the link between intracranial and jugular-vertebral circuit, increases with change of posture from supine to upright in basal conditions (+2.68 mmHg) as shown in Fig. 8. In supine posture, total occlusion of right jugular vein ($G_{jr3} = 0$, $G_{jr2} = 0$, and $G_{jr1} = 0$) produces little increases of the value of P_{vs}. Also, changes due to occlusions of collateral network and vertebral veins are not appreciable. Conversely, looking at the simulation of upright condition, it is evident that P_{vs} is more influenced by lack of drainage of the collateral network ($G_{c3} = 0$), while all the other kinds of occlusion only affect P_{vs} with little or not appreciable increases.

Figure 9 shows that output flow from the confluence of jugular veins Q_{svc1} decreases of about −3.1 ml/s from the supine to upright condition. In supine condition, every kind of occlusion evokes little or negligible changes of this flow. The same situation also occurs in upright condition.

Output flow from the vertebral veins Q_{vv} rises of 2.6 ml/s during change from supine to upright conditions as reported in Fig. 10. Little variations from the basal supine value occur when a jugular vein is occluded. Conversely, basal upright flow is quite increased by occlusion of the collateral network ($G_{c3} = 0$) and lowered by occlusion of right vertebral vein ($G_{vvr} = 0$).

The most influential closure is found in the collateral circulation: in upright conditions it provokes a further increase in venous sinuses pressure up to ~10 mmHg and also a redistribution of blood flow toward the vertebral-azygos complex. Obstruction of a jugular vein is relevant especially when it occurs close to its terminal part, causing a reduction of jugular outflow down to 11.4 ml/s. Naturally, an obstruction in a vertebral vein causes a significant decline in vertebral blood flow, with a redistribution toward the jugular and collateral circulations.

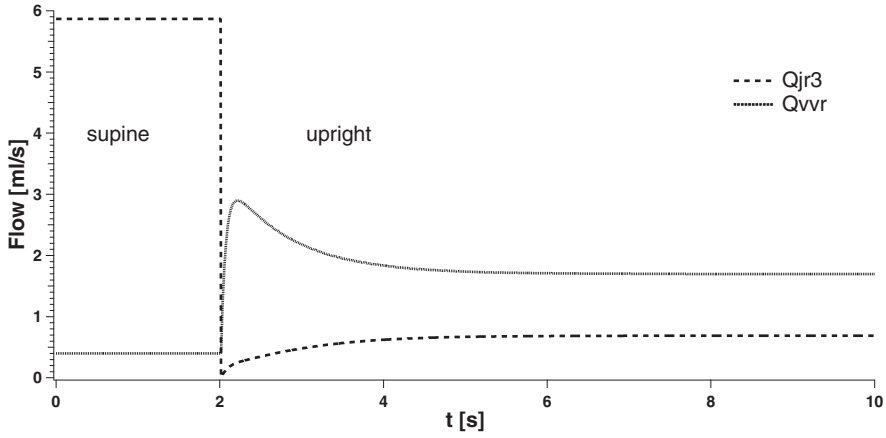

Fig. 6. Right jugular (Q_{jr3}) and vertebral (Q_{vvr}) flow behavior over time in supine and upright simulations.

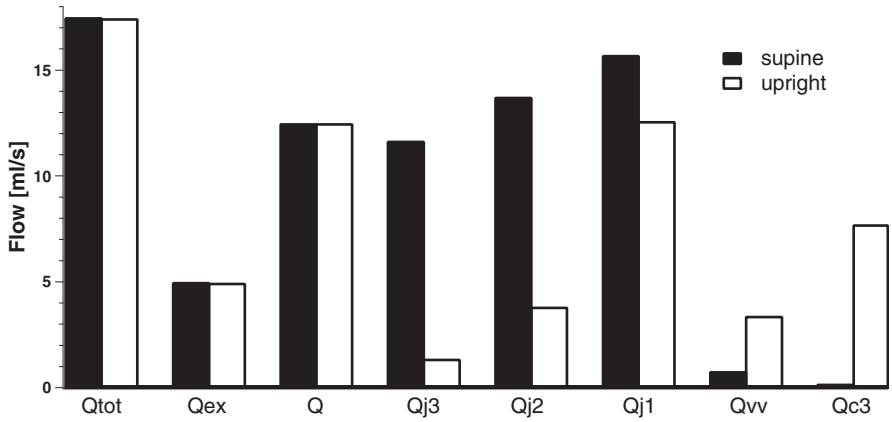

Fig. 7. Basal flows in supine and upright simulations.

Finally, we tested the behavior of the external flow Q_{ext} for all the conditions described above. In the present model Q_{ext} diminishes by 0.05 ml/s when venous sinuses pressure increases (for example, when moving from supine to upright condition both in a healthy and a pathological subject). This external flow is not significantly affected by any kind of occlusion we tested, apart for a little decrease during the occlusion of the lower jugular segment and a little increase during the occlusion of the collateral pathway c3 (-0.03 and $+0.02$ ml/s, respectively). We also performed the whole sensitivity analysis in the conditions of weak autoregulation reported in Fig. 2. Results show that for reduced cerebral autoregulation (i.e., by changing the value of G_{aut} till 1/10 of its initial value) every value of pressure and flow reported in the sensitivity analysis does not change significantly. The reason is that, in our simulations, venous sinuses pressure always exhibits a mild change ($+$ 1 or $+2$ mmHg), which is a minimal fraction of cerebral perfusion pressure. Since cerebral blood flow is subjected to regulation mechanisms, the final change in cerebral blood flow is always $<1\%$ of basal (even when using a moderate autoregulation gain), which has negligible effects on the final results.

Multiple occlusions. The effect of multiple occlusions may be much more dramatic. In the following, we will especially analyze the changes in venous sinuses pressure, since this quantity represents a link between the cerebral circulation and the extracranial venous outflow system. We report in Fig. 11 a histogram to show how the basal venous sinuses pressure P_{vs} varies when stenotic patterns occur. Together with the simulations of null conductance, we reported also the simulations of the same patterns but with halved conductances.

A more complete description can be found in Tables 5 and 6, which report results concerning blood flows and pressures redistribution due to the different stenotic patterns described in Ref. 39, compared with the simulation of a healthy distribution.

Pattern A refers to simulation of obstruction of the proximal azygos azy2, associated with a closed stenosis of the left internal jugular vein. Pattern B refers to simulation of obstructions of both the internal jugular veins and the proximal azygos. Pattern C refers to simulation of obstructions of both the internal jugulars but without stenoses in the azygos system. Finally, pattern D refers to simulation of obstructions in different tracts of the azygos vein (azy1 and azy2) associated with occlusion of the lumbar vein.

Results show that two particular pathological patterns (i.e., patterns B and C) may have a strong effect on venous sinuses pressure, which reaches values as high as 13–16 mmHg both in supine and upright positions. Such value may have consequences on intracranial pressure, cerebrospinal fluid circulation, and cerebral tissue. However, this pressure increase occurs only if the stenotic lesions are very severe (conductances close to zero). Moderate levels of conductance changes, although multiple, cause more acceptable pressure rises.

For what concerns model validation, we cannot use animal data taken from the literature, as usually done, since the extracranial venous drainage pathways are significantly different in animals compared with humans. In particular, the extracranial venous circulation in humans is specifically adapted

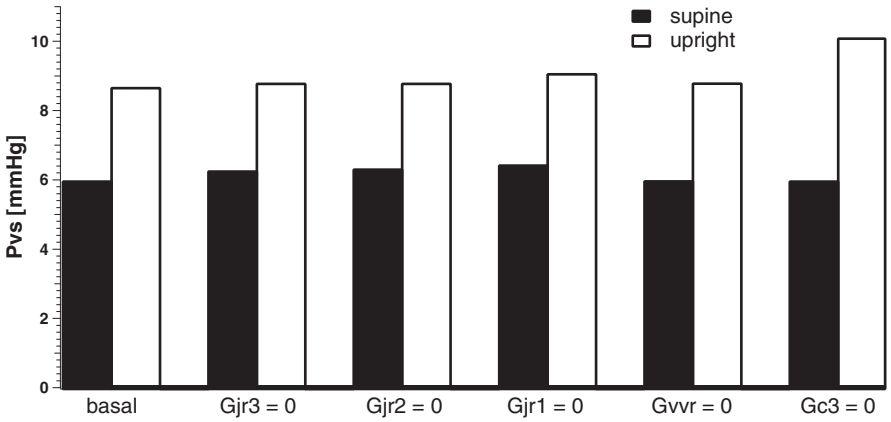

Fig. 8. Sensitivity analysis of venous sinuses pressure (P_{vs}).

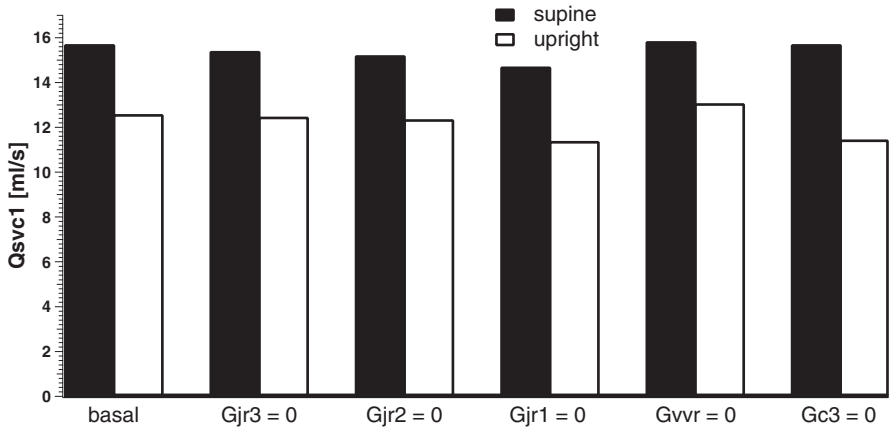

Fig. 9. Sensitivity analysis of jugular veins outflow (Q_{svc1}).

to the maintenance of an upright posture, which is the peculiar subject of the present work. For this reason, we are designing some ad hoc measurements on volunteers, using the Doppler technique, to assess blood flow changes and cross-sectional areas in the different portions of the jugular veins and to provide a complete quantitative set for model validation (or for discovering aspects requiring improvement). This will be the subject of a future work. When imaging with the current diagnostic methods multiple stenotic patterns or flow abnormalities in the major extracranial and extraspinal veins, which are typical of chronic cerebrospinal venous insufficiency (CCSVI), it is difficult to confidently assign their hemodynamic significance for the intracranial circulation. It has been recently emphasized that the main issue to be investigated in this field is the definition of the hemodynamic impact in the intracranial venous system of obstruction/narrowing of the extracranial veins (46). Since, at this time, there is no established invasive or noninvasive diagnostic imaging modality capable to assess intracranial and/or parenchymal circulatory parameters in relation to extracranial brain outflow (47), the clinical application of the present model seems highly desirable. For instance, in the present study we tested our model on four clinical patterns of extracranial venous obstruction, clinically detected in patients by means of catheter venography (39). In Fig. 11, we report the estimated pressure values in the cerebral dural sinuses in relation to the different CCSVI patterns. The application of the model demonstrates a significant increase of venous sinuses pressure especially for type B and C but not in patterns A and D. Such a result appears to be coherent with the clinical severity and/or the topography of multiple sclerosis, the neurological disease associated with the observed patterns of venous obstruction in this cohort of patients. As far as the severity is concerned, patients with type A pattern (characterized by reduced sinusal pressure) demonstrated, with respect to B and C patterns, a significantly reduced probability to worsen to the secondary progressive clinical stage (39). Regarding the topography of the lesions in the central nervous system, type D pattern exhibits few cerebral lesions and prevalent MRI plaque dissemination in the spinal cord (39). Speculatively, this result suggests that increased pressure in the cerebral sinuses may clinically influence either the disease progression or the topography of multiple sclerosis plaques and warrants further studies in this direction.

Conclusions

We developed a lumped mathematical model for the study of cerebral venous outflow, able to simulate the average blood flows in the main drainage vessels of the brain. The two main features of the model are that it accounts for the dependence of the hydraulic properties of the jugular veins with respect to the gravity field and that it includes a validated model for the simulation of the intracranial circulation. That makes it an useful tool for the study of the correlations between extracra-

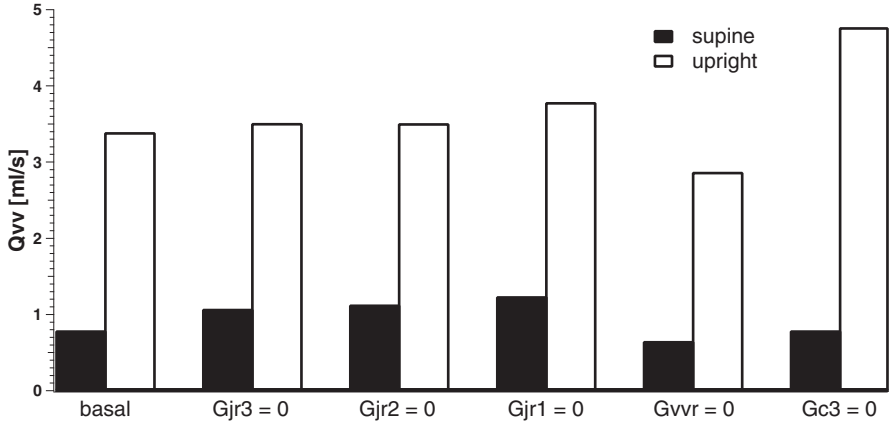

Fig. 10. Sensitivity analysis of vertebral veins outflow (Q_{vv}).

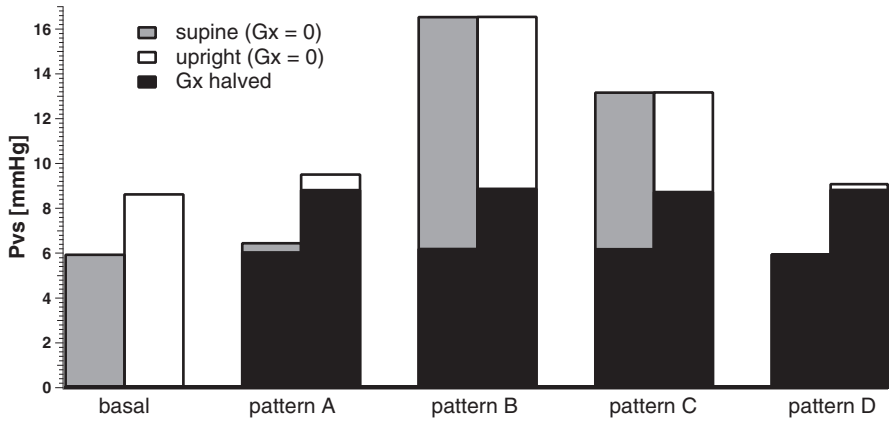

Fig. 11. Venous sinuses pressure P_{vs} in healthy and stenotic patterns simulation. The black columns represent the simulation of stenotic patterns with halved conductances with respect to the basal values.

nial blood redistributions and changes in the intracranial environment.

We performed simulations of the effect of posture change from supine to upright on pressures and blood flows, first with basal drainage and then assuming a lack of conductance of some particular vessel tract.

Results show that the model is able to reproduce the average physiologic behavior of the jugular, vertebral, and cerebral ducts, with values in good agreement with literature data. In addition to that, the model is able to give information about the average flows in different points of the jugular ducts, so taking into account the amount of blood coming from the anastomotic connections.

Moreover, we can easily use it to verify how the blood redistribution due to change of posture affects the pressures in specific points of the system.

We are aware only of a previous model that investigates cerebral venous return in accurate quantitative terms (14). The present model shows some similarities with that model, but it also exhibits many important new aspects.

First, the description of the cerebral venous return now includes a larger number of drainage pathways encompassing not only the vertebral one but also additional collateral and anastomoses to the downstream jugular sections. Inclusion of such a more complex network of collaterals is important to simulate several experimental observations. Basically, blood flow measurements show that the sum of the jugular and vertebral blood flows decrease from supine to upright position (33). This result is in contradiction with the existence of strong autoregulation mechanisms in the brain, which maintain quite a constant cerebral blood flow despite moderate pressure changes, and reveals the existence of further collateral routes beside the vertebral veins, able to drain cerebral blood flow in the erect position. Furthermore, measurements with the Doppler technique show that the amount of blood flow in the jugular veins increases from the upstream to the downstream sections (6, 8, 10, 28, 33, 41, 44), a result that requires the presence of anastomoses, which allow a progressive reentry of blood flow.

The second new aspect of the model consists in the strict link between the cerebral circulation (with its regulatory mechanisms), the cerebrospinal fluid circulation, and the cerebral venous return system.

Indeed, previous models were just devoted to study the cerebral venous return without paying attention to the cerebral circulation [Gisolf et al. (14)]. Other models were especially devoted to brain circulation and cerebral blood flow control with just an approximate description of the venous return, as for example in Ursino and Lodi (30). We claim that a model that incorporates both aspects is necessary, since the interconnections between the cerebral circulation and venous return systems may have important hemodynamics effects, especially in pathological conditions. In particular, the presence of regulatory mechanisms able to maintain a constant cerebral blood flow even when cerebral perfusion pressure falls down to

Table 5. *Venous sinuses pressure and intracranial pressure at equilibrium in simulation of basal conditions and typical stenotic patterns*

Pressure, mmHg	Basal	Pattern A	Pattern B	Pattern C	Pattern D
Supine					
P_{vs}	5.98	6.51	16.60	13.22	6.01
P_{ic}	9.44	9.51	11.09	9.95	9.44
Upright					
P_{vs}	8.68	9.57	16.55	13.23	9.14
P_{ic}	9.81	9.93	11.12	9.95	9.87

Table 6. *Flows at equilibrium in simulation of basal conditions and typical stenotic patterns*

Flow, ml/s	Basal	Pattern A	Pattern B	Pattern C	Pattern D
Supine					
Q_{vv}	0.79	0.51	3.86	7.86	0.33
Q_{jr3}	5.87	11.14	3.04	2.13	6.08
Q_{jl3}	5.87	0.81	3.04	2.13	6.08
Q_{jr2}	6.87	12.90	2.98	1.86	7.08
Q_{jl2}	6.87	0.88	2.98	1.86	7.08
Q_{jr1}	7.86	15.39	0.00	0.00	8.08
Q_{jl1}	7.86	0.00	0.00	0.00	8.08
Q_{svc1}	15.72	15.39	0.00	0.00	16.16
Q_{c1}	1.00	1.57	12.98	9.24	1.01
Q_{totout}	17.50	17.47	16.91	17.10	17.50
Upright					
Q_{vv}	3.39	1.54	3.64	7.87	1.37
Q_{jr3}	0.69	1.62	1.14	2.10	1.10
Q_{jl3}	0.69	1.32	1.14	2.10	1.10
Q_{jr2}	1.92	4.99	2.95	1.84	2.48
Q_{jl2}	1.92	1.62	2.95	1.84	2.48
Q_{jr1}	6.30	13.38	0.00	0.00	7.24
Q_{jl1}	6.30	0.00	0.00	0.00	7.24
Q_{svc1}	12.59	13.38	0.00	0.00	14.48
Q_{c1}	1.46	2.48	12.97	9.23	1.59
Q_{totout}	17.45	17.40	16.91	17.10	17.44

50–60 mmHg might produce large increases in venous sinuses pressure, if the venous return system becomes unable to drain all the required amount of blood flow.

The present simulations suggest two important considerations. The cerebral venous return system is quite robust: a single occlusion, or even multiple occlusions of moderate entity, can induce only mild changes in venous sinuses pressure and in total blood flow. Indeed, this is the fundamental role of the strong anastomotical connections incorporated in the model. However, we have also shown that pathological states, characterized by multiple severe obstructions, can lead to significant pressure changes in the venous sinuses, hence, in possible alteration in cerebrospinal fluid circulation and brain tissue pressure. Which adjustments may be produced in these cases (either the opening of new collaterals, a reset of the autoregulation set point, or a permanent pressure increase) remains to be investigated.

A final important aspect of the model consists in the possibility to simulate the progressive increase in jugular blood flow when moving from the upstream sections close to the skull to the downstream sections in the thoracic portion. These changes are amplified by a posture change, when the different sections of the jugular veins experience a different amount of collapse and are significantly affected by any individual or pathological alteration in the collateral pathways.

Hence, a study of these blood flow variations, for instance via quantitative Doppler measurements, may represent a strong test to validate the model and to adapt its parameters to individual characteristics.

APPENDIX

Intracranial Circuit

Mathematical equations for intracranial blood dynamics and cerebrospinal fluid circulation have been written by imposing the mass preservation principle at all the circuit nodes.

In the following, we refer to resistance of a given tract R_x as the inverse of the conductance G_x of the same tract. Table A1 provides a glossary of terms.

Mass preservation at the node of pial arterioles pa implies the following equation:

$$\frac{\mathrm{d}(\mathrm{P_{pa}}-\mathrm{P_{ic}})}{\mathrm{d}t}=\frac{1}{C_{\mathrm{pa}}}\left[\frac{\mathrm{P_a}-\mathrm{P_{pa}}}{R_{\mathrm{la}}+R_{\mathrm{pa}}/2}-\frac{\mathrm{P_{pa}}-\mathrm{P_c}}{R_{\mathrm{pa}}/2}-\frac{\mathrm{d}C_{\mathrm{pa}}}{\mathrm{d}t}(\mathrm{P_{pa}}-\mathrm{P_{ic}})\right] \quad (3)$$

Capillary pressure $\mathrm{P_c}$ is given by:

$$\mathrm{P_c}=\left(\frac{\mathrm{P_v}}{R_{\mathrm{pv}}}+\frac{\mathrm{P_{pa}}}{R_{\mathrm{pa}}/2}+\frac{\mathrm{P_{ic}}}{R_{\mathrm{f}}}\right)\Big/\left(\frac{1}{R_{\mathrm{pv}}}+\frac{1}{R_{\mathrm{pa}}/2}+\frac{1}{R_{\mathrm{f}}}\right) \quad (4)$$

The left term of *Eq. 3* is the variation of transmural pressure in time at the node of pial arterioles. It depends on the blood flow entering and leaving the node (the first 2 terms in the brackets at the right side) and on the active changes in arterial capacity C_{pa} over time (the last term in brackets). The value of C_{pa} at the denominator accounts for the ability of the duct to store blood without variations of transmural pressure: the higher the value of C_{pa} the lower the change in pressure over time. All other mass preservation equations have a similar meaning.

Mass preservation at the node of cerebral veins vi implies the following equation:

$$\frac{\mathrm{d}(\mathrm{P_v}-\mathrm{P_{ic}})}{\mathrm{d}t}=\frac{1}{C_{\mathrm{vi}}}\left[\frac{\mathrm{P_c}-\mathrm{P_v}}{R_{\mathrm{pv}}}-\frac{\mathrm{P_v}-\mathrm{P_{vs}}}{R_{\mathrm{vs}}}\right] \quad (5)$$

The relationship between C_{vi} and pressure is given by the following equation:

$$C_{\mathrm{vi}}=\frac{1}{k_{\mathrm{vcn}}(\mathrm{P_v}-\mathrm{P_{ic}}-\mathrm{P_{v1}})} \quad (6)$$

Control mechanisms work at the level of the arteriolar cerebrovascular bed by modifying R_{pa} and C_{pa}. Autoregulation activated by relative changes in cerebral blood flow Q is given by the following equation:

$$\frac{\mathrm{d}x_{\mathrm{aut}}}{\mathrm{d}t}=\left(\frac{1}{\tau_{\mathrm{aut}}}\right)\left[-x_{\mathrm{aut}}+G_{\mathrm{aut}}\left(\frac{\mathrm{Q}-\mathrm{Q_n}}{\mathrm{Q_n}}\right)\right] \quad (7)$$

where the minus sign of x_{aut} simulates the fact that a fall in blood flow causes a rapid dilatation of resistance vessels, whereas a rise in blood pressure causes vasoconstriction.

The existence of maximal limits for the vascular response (total vasodilation and maximal vasoconstriction) is simulated by a sigmoidal relationship with upper and lower saturation levels acting on pial arteries capacity C_{pa}, so that:

$$C_{\mathrm{pa}}=\frac{\left(C_{\mathrm{pa_n}}-\frac{\Delta C_{\mathrm{pa}}}{2}\right)+\left(C_{\mathrm{pa_n}}+\frac{\Delta C_{\mathrm{pa}}}{2}\right)\exp\left[\frac{-x_{\mathrm{aut}}}{kC_{\mathrm{pa}}}\right]}{1+\exp\left[\frac{-x_{\mathrm{aut}}}{kC_{\mathrm{pa}}}\right]} \quad (8)$$

The sigmoidal curve cannot be symmetrical because the increase in blood volume induced by vasodilation is higher than the blood volume decrease induced by vasoconstriction. Hence, two different values must be chosen for the parameter ΔC_{pa}, depending on whether vasodilation or vasoconstriction is considered. We have

$$\text{if } x_{\mathrm{aut}}<0 \text{ then } \Delta C_{\mathrm{pa}}=\Delta C_{\mathrm{pa1}} \text{ and } kC_{\mathrm{pa}}=\Delta C_{\mathrm{pa1}}/4 \quad (9)$$

for the vasodilation simulation, and

$$\text{if } x_{\mathrm{aut}}>0 \text{ then } \Delta C_{\mathrm{pa}}=\Delta C_{\mathrm{pa2}} \text{ and } kC_{\mathrm{pa}}=\Delta C_{\mathrm{pa2}}/4 \quad (10)$$

for the vasoconstriction simulation.

The value of pial arterioral resistance is given by the formula:

$$R_{\mathrm{pa}}=\frac{k_R C_{\mathrm{pan}}^2}{\left[(\mathrm{P_{pa}}-\mathrm{P_{ic}})C_{\mathrm{pa}}\right]^2} \quad (11)$$

The following equations account for cerebrospinal fluid formation rate $\mathrm{Q_f}$ and outflow rate $\mathrm{Q_0}$

$$\mathrm{Q_f}=\frac{\mathrm{P_c}-\mathrm{P_{ic}}}{R_{\mathrm{f}}} \text{ if } \mathrm{P_c}>\mathrm{P_{ic}}, \text{ else } \mathrm{Q_f}=0 \quad (12)$$

$$\mathrm{Q_0}=\frac{\mathrm{P_{ic}}-\mathrm{P_{vs}}}{R_0} \text{ if } \mathrm{P_{ic}}>\mathrm{P_{vs}}, \text{ else } \mathrm{Q_0}=0 \quad (13)$$

An expression for the resistance of the terminal intracranial veins R_{vs} is computed as follows:

$$R_{\mathrm{vs}}=\frac{\mathrm{P_v}-\mathrm{P_{vs}}}{\mathrm{P_v}-\mathrm{P_{ic}}}R_{\mathrm{vs1}} \text{ if } \mathrm{P_v}>\mathrm{P_{vs}}, \text{ else } R_{\mathrm{vs}}=R_{\mathrm{vs1}} \quad (14)$$

Application of mass preservation at the intracranial volume leads to the following equations:

$$\frac{\mathrm{dP_{ic}}}{\mathrm{d}t}=\frac{1}{C_{\mathrm{ic}}}\left[\frac{\mathrm{d}(\mathrm{P_{pa}}-\mathrm{P_{ic}})}{\mathrm{d}t}C_{\mathrm{pa}}+\frac{\mathrm{d}(\mathrm{P_v}-\mathrm{P_{ic}})}{\mathrm{d}t}C_{\mathrm{vi}}+\frac{\mathrm{d}C_{\mathrm{pa}}}{\mathrm{d}t}(\mathrm{P_{pa}}-\mathrm{P_{ic}})+\mathrm{Q_f}-\mathrm{Q_0}+\mathrm{hbf}\right] \quad (15)$$

and

Table A1. *Glossary of terms*

Symbol	Quantity	Symbol	Quantity	Symbol	Quantity	Symbol	Quantity
A	Parameter related to the resistance of the jugular segments to collapse	C_{azy}	Capacity of the azygos system	C_{pa}	Capacity of the pial arterioles	ΔC_{pa}	Amplitude of the curve of the pial arterioles capacity
AZY	Lumbo-azygos system	C_{c2}	Capacity of the middle segment of the collateral network	C_{pan}	Basal capacity of the pial arterioles	ΔC_{pa1}	Value of the capacity of the pial arterioles during vasodilation simulation
azy1	Distal azygos	C_{c3}	Capacity of the upper segment of the collateral network	CSF	Cerebrospinal fluid	ΔC_{pa2}	Value of the capacity of the pial arterioles during vasoconstriction simulation
azy2	Proximal azygos	C_{ic}	Intracranial capacity	C_{svc}	Capacity of the superior vena cava	g	Gravity acceleration
c3	Upper segment of the collateral network	C_{jl2}	Capacity of the middle segment of the left jugular vein	C_{vi}	Capacity of the intracranial veins	G_0	Conductance of the cerebrospinal fluid outflow tract
CBF	Cerebral blood flow	C_{jl3}	Capacity of the upper segment of the left jugular vein	C_{vs}	Capacity of the terminal intracranial veins	G_{aut}	Gain of the autoregulation mechanism related to CBF variations
cj2	Lower anastomoses	C_{jr2}	Capacity of the middle segment of the right jugular vein	C_{vv}	Capacity of the vertebral veins	G_{azy1}	Conductance of the distal azygos
cj3	Upper anastomoses	C_{jr3}	Capacity of the upper segment of the right jugular vein	C_x	Capacity of the generic segment x of the circulatory system	G_{azy2}	Conductance of the proximal azygos
G_{c1}	Conductance of the lower segment of the collateral network	G_{ex}	Conductance of the external carotid arteries	G_{lv}	Conductance of the lumbar vein	G_x	Conductance of the generic segment x of the circulatory system
G_{c2}	Conductance of the middle segment of the collateral network	G_{jl1}	Conductance of the lower segment of the left jugular vein	G_{svc1}	Conductance of the upper segment of the superior vena cava (jugular confluence)	h	Length of a jugular segment
G_{c3}	Conductance of the upper segment of the collateral network	G_{jl2}	Conductance of the middle segment of the left jugular vein	G_{svc2}	Conductance of the lower segment of the superior vena cava	hbf	Mock cerebrospinal fluid possibly injected into or subtracted from the cranial cavity
G_{cjl2}	Conductance of the lower anastomotic connection (left side)	G_{jl3}	Conductance of the upper segment of the left jugular vein	G_{vs}	Conductance of the terminal intracranial veins	IJV	Internal jugular vein
G_{cjl3}	Conductance of the upper anastomotic connection (left side)	G_{jr1}	Conductance of the lower segment of the right jugular vein	G_{vv2}	Conductance of the lower part of the vertebral vein	J1	Lower segment of the internal jugular veins
G_{cjr2}	Conductance of the lower anastomotic connection (right side)	G_{jr2}	Conductance of the middle segment of the right jugular vein	G_{vvl}	Conductance of the left vertebral vein	J2	Middle segment of the internal jugular veins
G_{cjr3}	Conductance of the upper anastomotic connection (right side)	G_{jr3}	Conductance of the upper segment of the right jugular vein	G_{vvr}	Conductance of the right vertebral vein	J3	Upper segment of the internal jugular veins
jr3	Upper segment of the right jugular vein	k_{jr2}	Parameter for the basal conductance of the middle segment of the right jugular vein	P_{azy}	Pressure in the azygos system	P_{j1ext}	Pressure outside the lower segment of the jugular veins
k_{Cpa}	Parameter for the capacity of the pial arterioles	k_{jr3}	Parameter for the basal conductance of the upper segment of the right jugular vein	P_c	Pressure in the intracranial capillaries	P_{j2ext}	Pressure outside the middle segment of the jugular veins
k_E	Intracranial elastance coefficient	k_R	Parameter for the resistance of pial arterioles	P_{c2}	Pressure in the middle segment of the collateral network	P_{j3ext}	Pressure outside the upper segment of the jugular veins
k_{jl1}	Parameter for the basal conductance of the lower segment of the left jugular vein	k_{ven}	Parameter for the intracranial venous capacity	P_{c3}	Pressure in the upper segment of the collateral network	P_{jl2}	Pressure in the middle segment of the left jugular vein
k_{jl2}	Parameter for the basal conductance of the middle segment of the left jugular vein	k_x	Parameter for the basal conductance of jugular and vertebral veins	P_{cv}	Pressure in the vena cava	P_{jl3}	Pressure in the upper segment of the left jugular vein
k_{jl3}	Parameter for the basal conductance of the upper segment of the left jugular vein	pa	Pial arterioles	P_{ic}	Intracranial pressure	P_{jr2}	Pressure in the middle segment of the right jugular vein

Continued

Table 1.—*Continued*

Symbol	Quantity	Symbol	Quantity	Symbol	Quantity	Symbol	Quantity
k_{jr1}	Parameter for the basal conductance of the lower segment of the right jugular vein	P_a	Arterial pressure	P_{icn}	Basal intracranial pressure	P_{jr3}	Pressure in the upper segment of the right jugular vein
P_{lv}	Pressure in the lumbar vein	P_{vv}	Pressure in the vertebral veins	Q_{c1}	Flow in the lower segment of the collateral network	Q_{ex}	Flow in the external carotid arteries (flow to face and neck)
P_{pa}	Pressure in the pial arterioles	P_x	Pressure in the generic segment x of the internal jugular veins	Q_{c2}	Flow in the middle segment of the collateral network	Q_f	Cerebrospinal fluid formation rate
P_{svc}	Pressure in the lower segment of the superior vena cava	P_{xext}	External pressure of the x segment of the internal jugular veins	Q_{c3}	Flow in the upper segment of the collateral network	Q_{j1}	Total flow in the lower segments of the jugular veins
P_{svc1}	Pressure in the upper segment of the superior vena cava (jugular confluence)	P_{xint}	Internal pressure of the x segment of the internal jugular veins	Q_{cjl2}	Flow in the lower anastomotic connection (left side)	Q_{j2}	Total flow in the middle segments of the jugular veins
P_v	Pressure in the cerebral veins	Q	Cerebral blood flow	Q_{cjl3}	Flow in the upper anastomotic connection (left side)	Q_{j3}	Total flow in the upper segments of the jugular veins
P_{v1}	Transmural pressure value at which cerebral veins collapse	Q_0	Cerebrospinal fluid outflow rate	Q_{cjr2}	Flow in the lower anastomotic connection (right side)	Q_{jl1}	Flow in the lower segment of the left jugular vein
P_{vs}	Pressure in the venous sinuses	Q_{azy1}	Flow in the distal azygos	Q_{cjr3}	Flow in the upper anastomotic connection (right side)	Q_{jl2}	Flow in the middle segment of the left jugular vein
Q_{jl3}	Flow in the upper segment of the left jugular vein	Q_{svc1}	Flow in the upper segment of the superior vena cava (jugular confluence)	R_f	Resistance to the cerebrospinal fluid formation	R_{vs1}	Terminal intracranial vein resistance when P_{ic} is equal to P_{vs}
Q_{jr1}	Flow in the lower segment of the right jugular vein	Q_{tot}	Total inflow	R_x	Resistance of the generic segment x of the circulatory system	t	Time
Q_{jr2}	Flow in the middle segment of the right jugular vein	Q_{totout}	Total outflow	ρ	Blood density	τ_{aut}	Time constant of the autoregulation mechanism related to cerebral flow variations
Q_{jr3}	Flow in the upper segment of the right jugular vein	Q_{vv}	Total flow in the vertebral veins	R_{la}	Resistance of the basal intracranial arteries	vi	Cerebral veins
Q_{lv}	Flow in the lumbar vein	Q_{vvl}	Flow in the left vertebral vein	R_{pa}	Resistance of the pial arterioles	VV	Vertebral vein
Q_n	Basal cerebral blood flow	Q_{vvr}	Flow in the right vertebral vein	R_{pv}	Resistance of the proximal intracranial veins	x	Generic segment of the circuit
Q_{rv}	Flow in the renal vein	R_0	Resistance to the cerebrospinal fluid outflow	R_{vs}	Resistance of the terminal intracranial veins	x_{aut}	State variable of the autoregulation mechanism related to cerebral flow variations

$$C_{ic} = \frac{1}{k_E P_{ic}} \quad (16)$$

This formula states that the variation in time of the intracranial pressure is the result of several factors. The first and the second term in brackets at the right side of *Eq. 15* refer to changes in transmural pressure at the level of arterioles and cerebral veins, the third term refers to change on pial artery capacity, while the other terms refer to cerebrospinal fluid inflow or outflow. Intracranial capacity C_{ic} at the denominator accounts for the ability of the skull to store volume.

Jugular-Vertebral Circuit

Mathematical equations for cerebral venous outflow simulation have been written by imposing the mass preservation principle at all the circuit nodes.

The state equations used to build the jugular-vertebral circuit are the following:

$$\frac{dP_{vs}}{dt} = \frac{1}{C_{vs}}\left[(P_v - P_{vs})G_{vs} - (P_{vs} - P_{ic})G_0 - (P_{vs} - P_{jr3})G_{jr3} - (P_{vs} - P_{jl3})G_{jl3} - (P_{vs} - P_{c3})G_{c3} - (P_{vs} - P_{vv})G_{vvl} - (P_{vs} - P_{vv})G_{vvr}\right] \quad (17)$$

$$\frac{dP_{jr3}}{dt} = \frac{1}{C_{jr3}}\left[(P_{vs} - P_{jr3})G_{jr3} - (P_{jr3} - P_{c3})G_{cjr3} - (P_{jr3} - P_{jr2})G_{jr2}\right] \quad (18)$$

$$\frac{dP_{jr2}}{dt} = \frac{1}{C_{jr2}}\left[(P_{jr3} - P_{jr2})G_{jr2} - (P_{jr2} - P_{c2})G_{cjr2} - (P_{jr2} - P_{svc1})G_{jr1}\right] \quad (19)$$

$$\frac{dP_{jl3}}{dt} = \frac{1}{C_{jl3}}\left[(P_{vs} - P_{jl3})G_{jl3} - (P_{jl3} - P_{c3})G_{cjl3} - (P_{jl3} - P_{jl2})G_{jl2}\right] \quad (20)$$

$$\frac{dP_{jl2}}{dt} = \frac{1}{C_{jl2}}\left[\left(P_{jl3} - P_{jl2}\right)G_{jl2} - \left(P_{jl2} - P_{c2}\right)G_{cjl2} - \left(P_{jl2} - P_{svc1}\right)G_{jl1}\right] \quad (21)$$

$$\frac{dP_{c3}}{dt} = \frac{1}{C_{c3}}\left[\left(P_{vs} - P_{c3}\right)G_{c3} + \left(P_{jr3} - P_{c3}\right)G_{cjr3} + \left(P_{jl3} - P_{c3}\right)G_{cjl3} + \left(P_{a} - P_{c3}\right)G_{ex} - \left(P_{c3} - P_{c2}\right)G_{c2}\right] \quad (22)$$

$$\frac{dP_{c2}}{dt} = \frac{1}{C_{c2}}\left[\left(P_{c3} - P_{c2}\right)G_{c2} + \left(P_{jr2} - P_{c2}\right)G_{cjr2} + \left(P_{jl2} - P_{c2}\right)G_{cjl2} - \left(P_{c2} - P_{cv}\right)G_{c1}\right] \quad (23)$$

$$\frac{dP_{svc}}{dt} = \frac{1}{C_{svc}}\left[\left(P_{svc1} - P_{svc}\right)G_{svc1} + \left(P_{azy} - P_{svc}\right)G_{azy2} - \left(P_{svc} - P_{cv}\right)G_{svc2}\right] \quad (24)$$

$$\frac{dP_{vv}}{dt} = \frac{1}{C_{vv}}\left[\left(P_{vs} - P_{vv}\right)G_{vvl} + \left(P_{vs} - P_{vv}\right)G_{vvr} - \left(P_{vv} - P_{azy}\right)G_{azy1} - \left(P_{vv} - P_{iv}\right)G_{vv2}\right] \quad (25)$$

$$\frac{dP_{azy}}{dt} = \frac{1}{C_{azy}}\left[\left(P_{vv} - P_{azy}\right)G_{azy1} + \left(P_{lv} - P_{azy}\right)G_{lv} - \left(P_{azy} - P_{svc}\right)G_{azy2}\right] \quad (26)$$

The equations used to include dynamics due to posture changes from supine to upright in the gravity field are the following:

$$G_{jr3} = k_{jr3}\left[1 + \left(\frac{2}{\pi}\right)\arctan\left(\frac{P_{vs} - P_{j3ext}}{A}\right)\right]^2 \quad (27)$$

$$G_{jl3} = k_{jl3}\left[1 + \left(\frac{2}{\pi}\right)\arctan\left(\frac{P_{vs} - P_{j3ext}}{A}\right)\right]^2 \quad (28)$$

$$G_{jr2} = k_{jr2}\left[1 + \left(\frac{2}{\pi}\right)\arctan\left(\frac{P_{jr3} - P_{j2ext}}{A}\right)\right]^2 \quad (29)$$

$$G_{jl2} = k_{jl2}\left[1 + \left(\frac{2}{\pi}\right)\arctan\left(\frac{P_{jl3} - P_{j2ext}}{A}\right)\right]^2 \quad (30)$$

$$G_{jr1} = k_{jr1}\left[1 + \left(\frac{2}{\pi}\right)\arctan\left(\frac{P_{jr2} - P_{j1ext}}{A}\right)\right]^2 \quad (31)$$

$$G_{jl1} = k_{jl1}\left[1 + \left(\frac{2}{\pi}\right)\arctan\left(\frac{P_{jl2} - P_{j1ext}}{A}\right)\right]^2 \quad (32)$$

GRANTS

This study was partially supported by the Italian Ministry of Education, University and Research (MIUR Programme PRIN 2010–2011) Grant No. 2010XE5L2R.

DISCLOSURES

No conflicts of interest, financial or otherwise, are declared by the author(s).

AUTHOR CONTRIBUTIONS

Author contributions: G.G., A.T., F.S., P.Z., and M.U. conception and design of research; G.G. performed experiments; G.G. analyzed data; G.G., A.T., F.S., and M.U. interpreted results of experiments; G.G. prepared figures; G.G., A.T., and M.U. drafted manuscript; G.G., A.T., F.S., M.G., P.Z., and M.U. edited and revised manuscript; G.G., A.T., F.S., M.G., P.Z., and M.U. approved final version of manuscript.

REFERENCES

1. **Aaslid R, Lindegaard KF, Sorteberg W, Nornes H.** Cerebral autoregulation dynamics in humans. *Stroke* 20: 45–52, 1989.
2. **Alperin N, Lee SH, Sivaramakrishnan A, Hushek SG.** Quantifying the effect of posture on intracranial physiology in humans by MRI flow studies. *J Magn Reson Imaging* 22: 591–596, 2005.
3. **Bassez S, Flaud P, Chauveau M.** Modeling of the deformation of flexible tubes using a single law: application to veins of the lower limb in man. *J Biomech Eng* 123: 58–65, 2001.
4. **Beggs CB.** Venous hemodynamics in neurological disorders: an analytical review with hydrodynamic analysis. *BMC Med* 11: 142, 2013.
5. **Braakman R, Sipkema P, Westerhof N.** A dynamic nonlinear lumped parameter model for skeletal muscle circulation. *Ann Biomed Eng* 17: 593–616, 1989.
6. **Chambers B, Chambers J, Churilov L, Cameron H, Macdonell R.** Internal jugular and vertebral vein volume flow in patients with clinically isolated syndrome or mild multiple sclerosis and healthy controls: results from a prospective sonographer-blinded study. *Phlebology* 29: 528–535, 2014.
7. **Cirovic S, Walsh C, Frases WD, Gulino A.** The effect of posture and positive pressure breathing on the hemodynamics of the internal jugular vein. *Aviat Space Environ Med* 74: 125–131, 2003.
8. **Doepp F, Paul F, Valdueza JM, Schmierer K, Schreiber SJ.** No cerebrocervical venous congestion in patients with multiple sclerosis. *Ann Neurol* 68: 173–183, 2010.
9. **Epstein HM, Linde HW, Crampton AR, Ciric IS, Eckenhoff JE.** The vertebral venous plexus as a major cerebral venous outflow tract. *Anesthesiology* 32: 332–337, 1970.
10. **Feng W, Utriainen D, Trifan G, Elias S, Sethi S, Hewett J, Haacke EM.** Characteristics of flow through the internal jugular veins at cervical C2/C3 and C5/C6 levels for multiple sclerosis patients using MR phase contrast imaging. *Neurol Res* 4: 802–809, 2012.
11. **Fontecave-Jallon J, Baconnier P.** Berkeley-Madonna implementation of Ikeda's model. *Conf Proc IEEE Eng Med Biol Soc* 2007: 582–585, 2007.
12. **Fung YC.** *Biomechanics Circulation*. New York: Springer, 1997.
13. **Giannessi M, Ursino M, Murray WB.** The design of a digital cerebrovascular simulation model for teaching and research. *Anesth Analg* 107: 1997–2008, 2008.
14. **Gisolf J, van Lieshout JJ, van Heusden K, Pott F, Stok WJ, Karemaker JM.** Human cerebral venous outflow pathway depends on posture and central venous pressure. *J Physiol* 560: 317–327, 2004.
15. **Grabe M, Oster G.** Regulation of organelle acidity. *J Gen Physiol* 117: 329–344, 2001.
16. **Guyton AC, Jones CE, Coleman TG.** *Circulatory Physiology: Cardiac Output and its Regulation*. London: WB Saunders, 1973.
17. **Karmon Y, Zivadinov R, Weinstock-Guttman B, Marr K, Valnarov V, Dolic K, Kennedy CL, Hojnacki D, Carl EM, Hagemeier J, Hopkins LN, Levy EI, Siddiqui AH.** Comparison of intravascular ultrasound with conventional venography for detection of extracranial venous abnormalities indicative of chronic cerebrospinal venous insufficiency. *J Vasc Interv Radiol* 24: 1487–1498.e1, 2013.

17a. **Macye RI, Oster GF.** *Berkeley Madonna* (Online). Univ. of California, Berkeley, CA. http://www.berkeleymadonna.com/jmadonna/jmadrelease.html [2001].

18. **Magosso E, Cavalcanti S, Ursino M.** Theoretical analysis of rest and exercise hemodynamics in patients with total cavopulmonary connection. *Am J Physiol Heart Circ Physiol* 282: H1018–H1034, 2002.
19. **Mancini M, Lanzillo R, Liuzzi R, Di Donato O, Ragucci M, Monti S, Salvatore E, Morra VB, Salvatore M.** Internal jugular vein blood flow in multiple sclerosis patients and matched controls. *PLoS One* 9: e92730, 2014.
20. **Olufsen MS, Ottesen JT, Tran HT, Ellwein LM, Lipsitz LA, Novak V.** Blood pressure and blood flow variation during postural change from sitting to standing: model development and validation. *J Appl Physiol* 99: 1523–1537, 2005.
21. **Paulson OB, Strandgaard S, Edvinsson L.** Cerebral autoregulation. *Cerebrovasc Brain Metab Rev* 2: 161–192, 1990.
22. **Piechnik SK, Czosnyka M, Harris NG, Minhas PS, Pickard JD.** A model of the cerebral and cerebrospinal fluid circulations to examine asymmetry in cerebrovascular reactivity. *J Cereb Blood Flow Metab* 21: 182–192, 2001.
23. **Press WH, Teukolsky SA, Vetterling WT, Flannery BP.** *Numerical Recipes in C*. New York: Cambridge Univ. Press, 1992.
24. **Radak D, Kolar J, Tanaskovic S, Sagic D, Antonic Z, Mitrasinovic A, Babic S, Nenezic D, Ilijevski N.** Morphological and haemodynamic abnormalities in the jugular veins of patients with multiple sclerosis. *Phlebology* 27: 168–172, 2012.
25. **San Millan Ruiz D, Gailloud D., Rufenacht DA, Delavelle J, Henry F, Fasel JH.** The craniocervical venous system in relation to cerebral venous drainage. *AJNR Am J Neuroradiol* 23: 1500–1508, 2002.

26. **Schaller B.** Physiology of cerebral venous blood flow: from experimental data in animals to normal function in humans. *Brain Res Brain Res Rev* 46: 243–260, 2004.
27. **Schreiber SJ, Lürtzing F, Götze R, Doepp F, Klingebiel R, Valdueza JM.** Extrajugular pathways of human cerebral venous blood drainage assessed by duplex ultrasound. *J Appl Physiol* 94: 1802–1805, 2003.
28. **Thibault P, Lewis W, Niblett S.** Objective duplex ultrasound evaluation of the extracranial circulation in multiple sclerosis patients undergoing venoplasty of internal jugular vein stenoses: a pilot study. *Phlebology* 2013 Dec 9 [Epub ahead of print].
29. **Traboulsee AL, Knox KB, Machan L, Zhao Y, Yee I, Rauscher A, Klass D, Szkup P, Otani R, Kopriva D, Lala S, Li DK, Sadovnick D.** Prevalence of extracranial venous narrowing on catheter venography in people with multiple sclerosis, their siblings, and unrelated healthy controls: a blinded, case-control study. *Lancet* 383: 138–145, 2014.
30. **Ursino M, Lodi CA.** A simple mathematical model of the interaction between intracranial pressure and cerebral hemodynamics. *J Appl Physiol* 82: 1256–1269, 1997.
31. **Ursino M, Magosso E.** Acute cardiovascular response to isocapnic hypoxia. I. A mathematical model. *Am J Physiol Heart Circ Physiol* 279: H149–H165, 2000.
32. **Ursino M, TerMinassian A, Lodi CA, Beydon L.** Cerebral hemodynamics during arterial and CO_2 pressure changes: in vivo prediction by a mathematical model. *Am J Physiol Heart Circ Physiol* 279: H2439–H2455, 2000.
33. **Valdueza JM, vonMünster T, Hoffman O, Schreiber S, Einhäupl KM.** Postural dependency of the cerebral venous outflow. *Lancet* 355: 200–201, 2000.
34. **Veroux P, Giaquinta A, Perricone D, Lupo L, Gentile F, Virgilio C, Carbonaro A, De Pasquale C, Veroux M.** Internal jugular veins outflow in patients with multiple sclerosis:a catheter venography study. *J Vasc Interv Radiol* 24: 1790–1797, 2013.
35. **Waite L.** *Biofluid Mechanics in Cardiovascular Systems*. New York: McGraw-Hill, 2006.
36. **Werner JD, Siskin GP, Mandato K, Englander M, Herr A.** Review of venous anatomy for venographic interpretation in chronic cerebrospinal venous insufficiency. *J Vasc Interv Radiol* 22: 1681–1690, 2011.
37. **Yazici B, Erdogmus, B, Tugay A.** Cerebral blood flow measurements of the extracranial carotid and vertebral arteries with Doppler ultrasonography in healthy adults. *Diagn Interv Radiol* 11: 195–198, 2005.
38. **Zamboni P, Consorti G, Galeotti R, Gianesini S, Menegatti E, Tacconi G, Carinci F.** Venous collateral circulation of the extracranial cerebrospinal outflow routes. *Curr Neurovasc Res* 6: 204–212, 2009.
39. **Zamboni P, Galeotti R, Menegatti E, Malagoni AM, Tacconi G, Dall'Ara S, Bartolomei I, Salvi F.** Chronic cerebrospinal venous insufficiency in patients with multiple sclerosis. *J Neurol Neurosurg Psychiatry* 80: 392–399, 2009.
40. **Zamboni P, Menegatti E, Occhionorelli S, Salvi F.** The controversy on chronic cerebrospinal venous insufficiency. *Veins Lymphatics* 2: 43–48, 2013.
41. **Zamboni P, Menegatti E, Pomidori L, Morovic S, Taibi A, Malagoni AM, Cogo AL, Gambaccini M.** Does thoracic pump influence the cerebral venous return? *J Appl Physiol* 112: 904–910, 2012.
42. **Zamboni P, Menegatti E, Weinstock-Guttman B, Schirda C, Cok JL, Malagoni AM, Hojnacki D, Kennedy C, Carl E, Dwyer MG, Bergsland N, Galeotti R, Hussein S, Bartolomei I, Salvi F, Ramanathan M, Zivadinov R.** CSF dynamics and brain volume in multiple sclerosis are associated with extracranial venous flow anomalies: a pilot study. *Int Angiol* 29: 140–148, 2010.
43. **Zamboni P, Morovic S, Menegatti E, Viselner G, Nicolaides AN.** Screening for chronic cerebrospinal venous insufficiency (CCSVI) using ultrasound- recommendations for a protocol. *Int Angiol* 30: 571–597, 2011.
44. **Zamboni P, Sisini F, Menegatti E, Taibi A, Malagoni AM, Morovic S, Gambaccini M.** An ultrasound model to calculate the brain blood outflow through collateral vessels: a pilot study. *BMC Neurol* 13: 81, 2013.
45. **Zaniewski M, Simka M.** Biophysics of venous return from the brain from the perspective of the pathophysiology of chronic cerebrospinal venous insufficiency. *Rev Recent Clin Trials* 7: 88–92, 2012.
46. **Zivadinov R, Chung CP.** Potential involvement of the extracranial venous system in central nervous system disorders and aging. *BMC Med* 11: 260, 2013.
47. **Zivadinov R, Bastianello S, Dake MD, Ferral H, Haacke EM, Haskal ZJ, Hubbard D, Liasis N, Mandato K, Sclafani S, Siddiqui AH, Simka M, Zamboni P.** Recommendations for multimodal noninvasive and invasive screening for detection of extracranial venous abnormalities indicative of chronic cerebrospinal venous insufficiency: a position statement of the international society for neurovascular disease. *J Vasc Interv Radiol* 25: 1785–1794.e17, 2014.